JGR | Machine Learning and Computation

RESEARCH ARTICLE
10.1029/2025JH000768

Real-Time Prediction of Salt Intrusion in Tidal Estuaries Using Long Short-Term Memory Networks

Karoline Rummel[1], Tobias Strauß[2], Franziska Lauer[3], and Ulf Gräwe[1]

[1]Leibniz Institute for Baltic Sea Research Warnemünde, Rostock, Germany, [2]Institute for Mathematics, University of Rostock, Rostock, Germany, [3]Federal Waterways Engineering and Research Institute, Hamburg, Germany

Key Points:

- Long Short-Term Memory networks enable real-time salt intrusion predictions, replicating numerical models with fast and accurate forecasts
- The method uses few observational inputs and works with missing data but depends on a well-calibrated numerical model for training
- Although long-term forecasts remain challenging, the approach demonstrates that model-derived variables can be predicted from observations

Correspondence to:

K. Rummel,
karoline.rummel@io-warnemuende.de

Citation:

Rummel, K., Strauß, T., Lauer, F., & Gräwe, U. (2025). Real-time prediction of salt intrusion in tidal estuaries using long short-term memory networks. *Journal of Geophysical Research: Machine Learning and Computation*, *2*, e2025JH000768. https://doi.org/10.1029/2025JH000768

Received 9 MAY 2025
Accepted 16 OCT 2025

Author Contributions:

Conceptualization: Ulf Gräwe
Formal analysis: Karoline Rummel
Methodology: Karoline Rummel, Tobias Strauß, Franziska Lauer, Ulf Gräwe
Visualization: Karoline Rummel
Writing – original draft: Karoline Rummel
Writing – review & editing: Tobias Strauß, Franziska Lauer, Ulf Gräwe

Abstract Estuaries worldwide provide unique ecosystems and critical freshwater resources for drinking water supply or agriculture. They are vulnerable to salt intrusion, which can have serious environmental and socioeconomic consequences. Obtaining a detailed picture of the state of the estuary through continuous monitoring is therefore essential. However, this is challenging due to the limited number of measurement stations. Numerical models provide such detailed insights but are computationally expensive and have limited suitability for real-time predictions. Data-driven models, such as Long Short-Term Memory (LSTM) networks, offer a promising alternative. In this study, LSTM networks are used to predict the location of the 2 g/kg bottom isohaline as an indicator for salt intrusion. Based on salinity, water level, wind, and river discharge data, the LSTM networks were trained on the salt intrusion length derived from a numerical model to estimate future salt intrusion accurately. Thus, detailed horizontal information from point measurements can be provided. This method is applied to the tidal Weser and Elbe estuaries, demonstrating that the network remains functional even when input stations are missing. Short-term environmental variability hampers longer-term forecasts, and limited data reduce prediction accuracy. Despite these constraints, our results show that LSTM networks replicate numerical model outputs from observational data and deliver real-time estimates of estuarine salt intrusion. This approach provides an efficient, adaptable tool for coastal monitoring and management.

Plain Language Summary Estuaries, where rivers meet the open seas, are unique ecosystems that often provide freshwater for drinking and agriculture. However, when the saltwater flows too far inland, the freshwater becomes unusable, making salt intrusion monitoring essential. Direct measurements are complex because measurement stations are often too far apart. Also, using computer models to simulate saltwater movement takes too long for real-time predictions. In this study, a type of artificial intelligence called Long Short-Term Memory (LSTM) networks is used to predict how far saltwater moves into estuaries. Different data types (such as salinity, water levels, wind, and river flow) are combined with computer model outputs to train LSTM networks. Once the network is trained, it is applied to the same data to predict saltwater movements quickly and accurately. The approach is tested on two tidal estuaries and shows that the network works even when some data is missing. However, predicting further into the future is more challenging because short-term events affect saltwater movement. This study shows that LSTM networks can make fast and accurate predictions of saltwater entering estuaries, helping with real-time monitoring and decision-making for coastal protection and water management.

1. Introduction

Salt intrusion is a growing threat to estuaries worldwide. With progressing climate change, the increased likelihood of droughts and the rising sea level create conditions favorable to intense salt intrusion (Bellafiore et al., 2021; Costa et al., 2023; Lee et al., 2024). The unique ecosystem of estuaries and the socioeconomic uses (e.g., fishery and freshwater abstraction for agricultural or drinking water purposes) are susceptible to changes in salinity. It is important to monitor changes to establish warning systems or response strategies.

For this purpose, real-time estimations of the salt intrusion are necessary. Establishing measurement stations for multiple parameters is an effective tool to provide real-time information at specific locations. However, the spatial distribution of those stations along an estuary is often sparse, impeding the ability to obtain comprehensive estimations of the entire estuary and the spatial dynamics. Numerical modeling has significantly advanced, providing detailed insights into the entire estuary. A notable disadvantage of such models is their need for extensive computing resources, making their application for real-time scenarios requiring high spatial and

temporal resolutions challenging and cost-intensive. Numerical models are often limited to a specific estuary and are hard to generalize. Consequently, alternative methods are needed to gather real-time estimations about salt intrusion into an estuary. Our suggested method requires only a numerical hindcast model run, real-time measurement data and could substitute numerical forecast models.

This study uses a data-driven approach, addressing this issue utilizing neural networks, particularly Long Short-Term Memory networks (LSTMs). Initially introduced by Hochreiter and Schmidhuber (1997), LSTMs display a further development of the classical recurrent neural networks (RNNs, Sherstinsky, 2020). Incorporating gating mechanisms within LSTMs helps to counteract the vanishing or exploding gradient problems that RNNs often face. The ability to "remember" crucial information from previous values has led to the frequent use of LSTMs in sequential applications, including natural language processing and time series analysis. In hydrodynamic applications, LSTMs have been successfully used for tasks such as predicting rainfall-runoff (Fang & Shao, 2022; Kratzert et al., 2018) or wave height (Jörges et al., 2021; Luo et al., 2022). Researchers have already applied random forests, feedforward neural networks, and support vector machines to predict estuarine salinity and salt intrusion (Alizadeh et al., 2018; Guillou et al., 2023; Hu et al., 2019; Rohmer & Brisset, 2017). More recently, they leveraged LSTM networks to forecast salinity dynamics in estuaries with high accuracy (Gorski et al., 2024; Saccotelli et al., 2024; Tian et al., 2024; Wang & Ge, 2025; Wullems et al., 2023; Zheng et al., 2024). However, earlier studies mainly focused on predicting salinity at specific locations instead of capturing the detailed estuarine salt-front dynamics that numerical models provide. Only two of the mentioned studies present approaches to estimate the spatial extent of salt intrusion. Tian et al. (2024) use LSTM networks and convolutional neural networks to predict the first principal component of an EOF analysis as a proxy for the severity of the salt intrusion in the Modaomen estuary. Gorski et al. (2024) estimate the location of the salt front in the Delaware Bay estuary solely based on observational data, as they are able to derive the target variable out of several measurement stations. They demonstrate better results than the available numerical model (COAWST). Nevertheless, they are only looking at the backward-looking 7-day average of the salt front. While most of the mentioned studies base their LSTM networks on measurement data, Wang and Ge (2025) utilize FVCOM numerical model output to get the input feature data.

In this study, we configure LSTM networks to predict the position of the 2 g/kg bottom isohaline. We derive this target from our numerical model and assemble the remaining input features from multiple monitoring stations. This strategy lets us reconstruct the salt intrusion frontal dynamics in detail using only real-time observations at fixed locations.

We applied our LSTM network to the tidal reaches of the Weser and Elbe estuaries in northern Germany. Although this method can be generalized to estuaries worldwide, these two systems exemplify highly dynamic salt intrusion fronts driven by tidal forcing and river discharge. Lauer and Kösters (2024) demonstrated that machine learning reliably predicts tidal extremes in the Weser estuary. In both estuaries, salt intrusion critically impacts the local ecosystem and limits freshwater abstraction for agriculture. During pumping periods, managers must keep salinity below predefined thresholds, so they rely on real-time monitoring to guide water withdrawals and coastal protection measures. A conductivity-based sensor network in the Elbe estuary has been installed to support irrigation scheduling as an early-warning system for elevated salinity (Waterways and Shipping Administration Hamburg, 2025). Although these stations are close, locating the salt intrusion front remains challenging, and our LSTM approach can bridge this gap using only observational data.

In this work, the LSTM networks provided a fast and accurate tool to provide information about the location and movement of the salt intrusion front in real time. This information could otherwise only be obtained through computationally expensive operational model simulations. Although the network is an offline application within the framework of this study, it has the potential to be integrated into online data flows to provide real-time prediction for interested parties. Section 4 presents and evaluates the corresponding performance of the LSTM networks. A detailed feature sensitivity study proved that the approach applies even in cases of interchanged or missing input data. We assess how input data quantity influences the LSTM networks' accuracy and demonstrate their ability to forecast up to one day ahead. Finally, we conclude our results in Section 5.

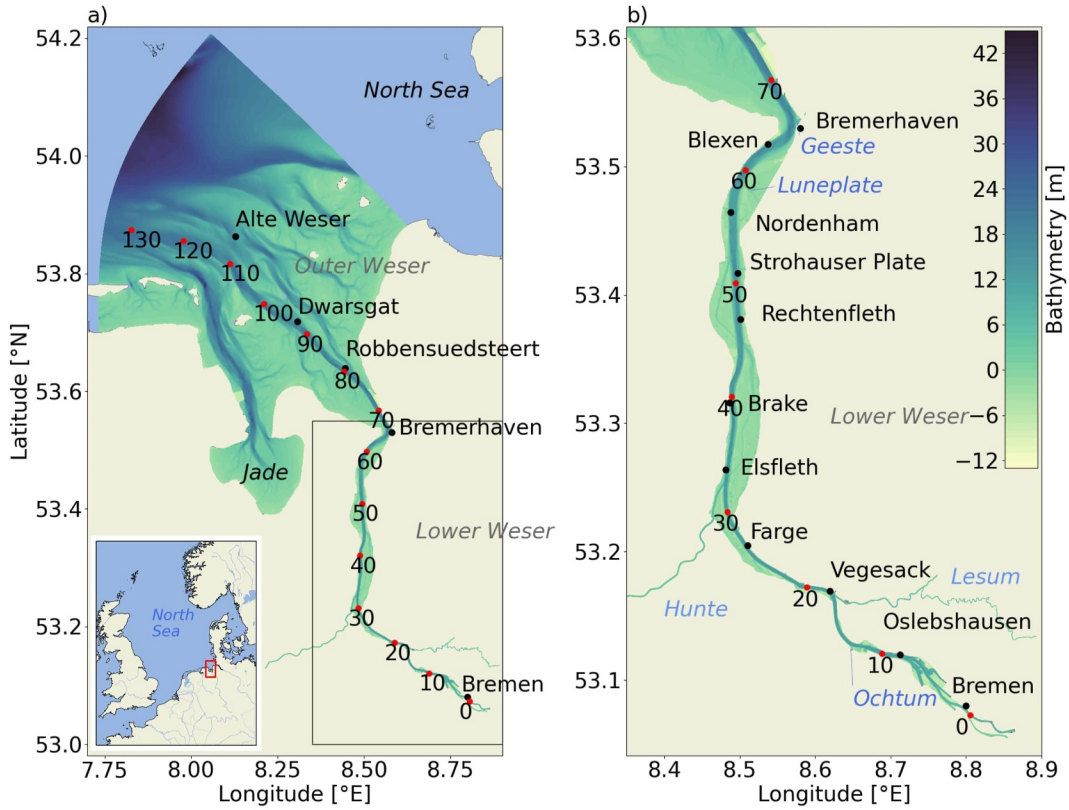

Figure 1. (a) The bathymetry is displayed inside the numerical model domain. Along the channel, the Weser km are marked with red dots, and the locations of measurement stations are highlighted with black dots. In the lower left, the model area is indicated with a red box on a map of northern Europe. The black box in the lower right corner shows the zoom for panel (b). Modified from Rummel et al. (2025).

2. Study Areas and Available Data

2.1. The Weser Estuary

The Weser estuary is located in north-west Germany, extending toward the North Sea. It consists of two main sections: the Outer Weser, stretching from the North Sea to Bremerhaven, and the Lower Weser, extending to the weir in Bremen, which marks the end of the tidal influence area. The estuary's hydrodynamics are strongly influenced by the tides and the freshwater inflow of the Weser River. The estuary is characterized by a deep navigational channel that connects the North Sea to major ports further upstream and is surrounded by tidal flat zones. The Weser estuary is classified as a partially to well mixed mesotidal estuary exhibiting a tidal range that varies from 2.8 m at the north of the Outer Weser up to 4.1 m in Bremen (Lange et al., 2008). The annual mean river discharge, measured at Intschede (approximately 30 km upstream of the weir), was 321 m^3s^{-1} during the period 1941–2015 (Niedersächsischer Landesbetrieb für Wasserwirtschaft, Küsten-und Naturschutz (NLWKN), 2015) with significant seasonal variability. The tides and the varying river discharge can both lead to differences in the salt intrusion length of up to 15–20 km (Kösters et al., 2014; Rummel et al., 2025) with the 2 g/kg bottom isohaline typically being located between Weser km 35–60. The Weser River enters the estuary with a salinity of approximately 0.5 g/kg as a consequence of upstream potash mining activities (Lange et al., 2008). Furthermore, smaller tributaries such as the Geeste, Lesum, Ochtum, and Hunte contribute relatively minor freshwater inflows to the estuary. The water of the Weser estuary is regularly abstracted for agricultural use, a practice that necessitates adherence to salinity limits.

2.1.1. Simulated Data

In this study, simulated data of a realistic Weser estuary numerical model setup as presented by Rummel et al. (2025) are used. The extent of the numerical model setup can be seen in Figure 1. The simulations utilize the

General Estuarine Transport Model (GETM, Burchard & Bolding, 2002), a three-dimensional numerical framework that solves the Reynolds-averaged Navier-Stokes equations under the Boussinesq approximation. The turbulence closure is achieved by coupling GETM with the General Ocean Turbulence Model (GOTM, Burchard et al., 1999), which applies a k-ε model using a second-order closure (Umlauf & Burchard, 2005). Tailored for applications in coastal ocean settings, GETM offers a robust tool for modeling complex estuarine and nearshore dynamics (Klingbeil et al., 2018). Detailed numerical model setup and validation information are shown by Rummel et al. (2025).

The simulation covers the period from 01.01.2015 to 01.01.2021. The length of the salt intrusion, which serves as the target variable, is estimated by determining the location of the 2 g/kg bottom isohaline in the channel. This calculation is simplified due to the curvilinear grid setup of the numerical model with one grid line always following the navigational channel. The model grid contains a total of 2,473 grid cells along the estuary and 592 cells in the cross-channel direction, leading to a channel resolution of about 50 m × 170 m near the northern boundary up to 7 m × 30 m close to Bremen. The temporal resolution of the model output is 1 hr.

2.1.2. Observational Data

Along the Weser estuary, 11 stations track water level and 10 stations track the salinity at a 1- or 5-min temporal resolution, respectively (Waterways and Shipping Administration Weser-Jade-Nordsee, 2024). The location of these stations can be seen in Figure 1.

The discharge of the Weser River is provided at a daily resolution at the station Intschede (Waterways and Shipping Administration Hann. Muenden, 2023) located approximately 30 km upstream of Bremen. Temperature and salinity information of the outflow are provided by the measurement station Hemelingen (Waterways and Shipping Administration Weser-Jade-Nordsee, 2023a) at the same resolution. The minor freshwater inflows of the tributaries Hunte, Lesum, Geeste and Ochtum are added to the total discharge (Waterways and Shipping Administration Weser-Jade-Nordsee, 2023b; Niedersächsischer Landesbetrieb für Wasserwirtschaft, Küsten-und Naturschutz (NLWKN) Verden, 2023).

Meteorological data, such as wind speed and direction, are provided by the German Meteorological Service (DWD) and are freely available from their Open Data Server (German Meteorological Service (DWD), 2025). We included hourly data from the station in Bremen.

2.2. The Elbe Estuary

The Elbe estuary is located less than 100 km to the east of the Weser estuary and is slightly larger than the latter. Due to their close proximity and related topographic characteristics, both estuaries show comparable salinity dynamics. In the Elbe estuary, which also opens to the North Sea, the tides dominate the salinity dynamics on a daily basis. Like the Weser estuary, the Elbe estuary is also characterized by a deep navigational channel surrounded by tidal flats. The Elbe estuary is classified as a partially to well mixed mesotidal estuary with a tidal range of about 2.9 m at Cuxhaven up to 3.7 m at Hamburg St. Pauli (Strotmann, 2014, 2015). The tidal influence extends upstream to the weir at Geesthacht. Compared to the Weser, the Elbe River discharge is notably higher with an annual mean discharge between 1926 and 2013 of 714 m^3/s (Strotmann, 2015), exhibiting strong variability. Several minor tributaries contribute to the total freshwater inflow into the estuary. For more details on the tributaries and their inclusion in the numerical model, see Reese et al. (2024). For the purpose of this study, the freshwater inflows of the tributaries are added to the total discharge.

In the Elbe, the salinity intrusion is dominated by the tides and changes in river discharge moving the end of the salt front on a kilometer scale—comparable to the Weser estuary. The usual position of the 2 g/kg isohaline is around Elbe km 85–110, but it can move further upstream under extreme conditions (Boehlich & Strotmann, 2008).

2.2.1. Simulated Data

Realistic simulated data for the Elbe estuary were available from 01.08.2012 to 01.01.2014. The setup was presented and validated by Reese et al. (2024). Like the Weser estuary, the simulation was also set up using a curvilinear grid and the GETM model. The resolution of the numerical model is slightly coarser with an average along-channel resolution of 200–400 m and an across-channel resolution mostly between 50 and 100 m. The

10.1029/2025JH000768

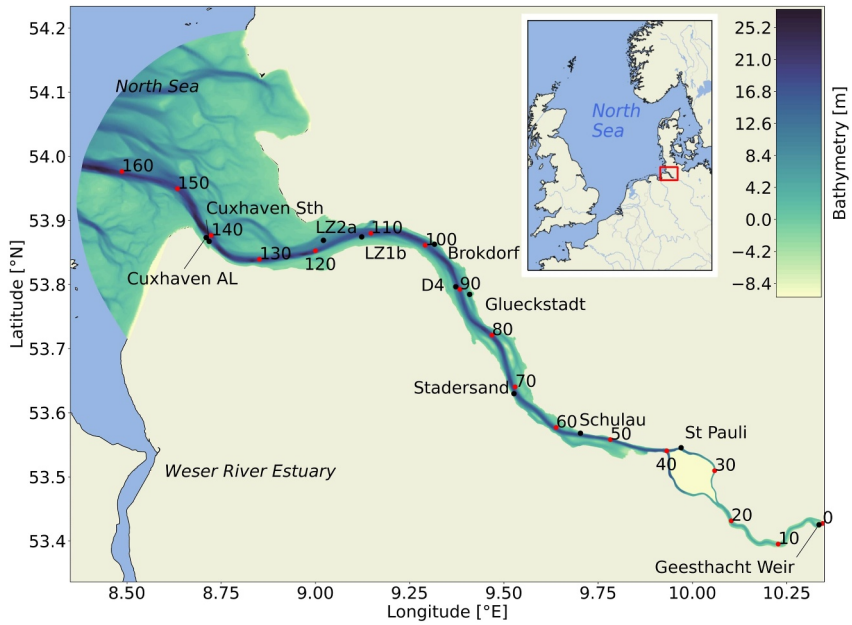

Figure 2. (a) The bathymetry is displayed inside of the numerical model domain. Along the channel, the Elbe km are marked with red dots, and the locations of measurement stations are highlighted with black dots. The model area is marked in a red box in a map of northern Europe.

model output is given at a 1 hour resolution. The salt intrusion length as a target variable was calculated similarly to the Weser estuary in Section 2.1.1.

2.2.2. Observational Data

Along the Elbe estuary, the data of 6 gauges and 4 salinity stations were available for the model simulation period (Waterways and Shipping Administration Elbe-Nordsee, 2025) and included in the latter. Further possible measurement stations could not be used because no corresponding simulated data existed in the available numerical model output. Otherwise, for applications at later periods, the data of more stations could be retrieved from the same source. The locations of the available stations are marked in Figure 2. The data have the same resolution as for the Weser estuary, namely 1 min for water level and 5 min for salinity.

The data for the river discharge are measured daily at station Neu Darchau, located 87 km upstream of Hamburg St. Pauli, which is the most upstream measurement station included in this study (Waterways and Shipping Administration Elbe, 2025). The salinity of the Elbe River discharge is assumed to be zero. Minor freshwater inflows from several tributaries are added to the total discharge, while only making up a small percentage of the freshwater inflow into the estuary. Wind strength and direction are given for the location Cuxhaven by the German Meteorological Service (DWD) (German Meteorological Service (DWD), 2025) at an hourly resolution.

3. Technical Details

3.1. Input Features

The machine learning algorithms were established based on different input features and the same target variable. As the target variable, we used the location of the 2 g/kg bottom isohaline in the navigational channel as a measure of the salt intrusion length.

We calculated the cross-correlation between the target variable's time series and each possible input feature to determine the input sequence length. We then selected the lag time at which the correlation peaked—30 hr—as our window size for both applications. During experiments in the model tuning phase, this choice could be

Table 1
Input Features Used for Training the LSTM Networks for the Weser and Elbe Estuaries

Feature type	Weser estuary	Elbe estuary
Water Level Stations	Robbensuedsteert, Elsfleth	Cuxhaven *S*th, Brokdorf, Schulau
Salinity Stations	Robbensuedsteert, Rechtenfleth, Elsfleth	Cuxhaven AL, LZ1b Krummendeich
River Discharge	Weser River + tributaries	Elbe River + tributaries
Wind	Bremen	Cuxhaven

confirmed as longer input sequence lengths did not increase the performance while increasing the computing time. Shorter windows tend to decrease the performance.

The network for the Weser estuary was trained on the 30 hr history of the water level at the stations "Robbensuedsteert" and "Elsfleth," the salinity of the stations "Robbensuedsteert", "Rechtenfleth" and "Elsfleth" as well as the discharge of the Weser River and the added tributaries and the wind direction and speed at station Bremen (see Figure 1). Although more measurement stations are available, this choice was sufficient for the network's performance. Adding more stations did not improve the network due to the high intercorrelation between the stations—we chose stations with a correlation of less than 0.8 (compare Figure A1). These findings indicate that when one station fails, we can substitute it with another station exhibiting a high correlation. We analyze this scenario in detail in Section 4.3. Furthermore, we tested the salinity of the Weser River discharge as an input feature, but it did not improve the model performance.

For the training of the network for the Elbe estuary, we used the 30 hr history of the water level stations "Cuxhaven Steubenhöft," "Brokdorf," and "Schulau," and the salinity at "Cuxhaven Alte Liebe" and "LZ1b Krummendeich" (see Figure 2), as for those stations the correlation was below 80%. As for the Weser estuary, the river discharge, including the tributaries, and the wind measurements at station Cuxhaven are used. Again, using more measurement stations did not lead to an increased performance. The input features of both networks are summarized in Table 1. The sensitivity of the choice of input features is further examined in Section 4.3.

We exclude autoregressive components (e.g., as in NARX networks) and never feed past target values into the network, so our predictions rely solely on observational inputs. Because we aim to replace the numerical model, we cannot use its historical outputs in our forecasts. Feeding the network's own predictions back into subsequent inputs would amplify errors.

Although the salt intrusion length is solely available as simulated data, the input features are chosen from (a) simulated data and (b) observational data. The simulated data inputs were taken as the numerical model results of the grid points closest to the measurement stations. Two exceptions are the river discharge and wind data only available as measured data. For both estuaries, we establish individual network structures. The network structure for each estuary is then first trained on simulated data and afterward on the stations' actual observational measurements to compare the performance. The performance with training on the simulated data is analyzed in Section 4.1 and with training on the actual measurements in Section 4.2.

3.2. Preprocessing

The LSTM network's input variables were standardized individually to have a mean μ of zero and a standard deviation σ of one. This is necessary to reduce the impact of the different magnitude scales of the input features and facilitate a stable and fast training process (see e.g., Sola & Sevilla, 1997). The standardized variable z for a variable x is calculated as follows:

$$z = \frac{x - \mu}{\sigma} \tag{1}$$

Furthermore, the input variables were adapted to the same temporal resolution as the target variable. Although the target variable from the simulation is available at every hour, most of the input variables were available at different resolutions. The wind measurements were available at the same time points, so they had the same temporal resolution and did not require modifications. For the higher-resolved salinity and water level

measurements, we used the instantaneous values at the specific time points. The only variable available at a lower resolution was the river discharge given as daily averages. In this case, we duplicated the daily values 24 times every hour to avoid including false information, for example, due to interpolation. Because daily averages vary only moderately, the network does not have to handle large, artificial jumps. Still, by this multiple duplication, subdaily discharge fluctuations could not be covered, which might bias the LSTM predictions during high-variability events.

3.3. Network Architecture

In this study, we established two LSTM network architectures to estimate the salt intrusion in both tidal estuaries. LSTM networks are a specific type of RNNs (RNN) presented by Hochreiter and Schmidhuber (1997) and designed to learn long-term dependencies in sequential data. Traditional RNNs only have one internal state: the hidden state h_t at time point t and suffer under the vanishing or exploding gradients problem when trained on longer sequences. The LSTM networks mitigate this limitation by introducing an additional memory vector: the cell state C_t. The cell state effectively stores state information and acts as a long-term memory. Implemented gating mechanisms control the information flow in the LSTM cell. At each time step t, the forget gate steers, which parts of the previous cell state C_{t-1} will be forgotten.

$$f_t = \sigma\left(W_f \cdot [h_{t-1}, x_t] + b_f\right) \tag{2}$$

with σ being the logistic sigmoid function, h_{t-1} the previous hidden state, x_t the current input vector and W_f and b_f learnable parameters. The input gate controls the contribution of the current input to the update of the cell state.

$$\begin{aligned} i_t &= \sigma(W_i \cdot [h_{t-1}, x_t] + b_i) \\ \tilde{C}_t &= \tanh(W_C \cdot [h_{t-1}, x_t] + b_C) \end{aligned} \tag{3}$$

with W_i, b_i, W_C, b_C being learnable parameters and $\tanh$ the hyperbolic tangent. The new cell state can then be computed by combining this information from the input gate with the previous cell state.

$$C_t = f_t \odot C_{t-1} + i_t \odot \tilde{C}_t \tag{4}$$

with $\odot$ denoting the Hadamard product (element wise multiplication). The third and last gate is the output gate that controls which information from the current cell state flow into the update of the hidden state. Lastly, the output gate defines how the updated cell state influences the update of the hidden state.

$$\begin{aligned} o_t &= \sigma(W_o \cdot [h_{t-1}, x_t] + b_o) \\ h_t &= o_t \odot \tanh(C_t) \end{aligned} \tag{5}$$

with W_o and b_o again being learnable parameters. With these implemented mechanisms, LSTM networks are able to capture long-term dependencies and learn temporal connections and are very suitable for prediction tasks. For further technical details on LSTM networks, see Hochreiter and Schmidhuber (1997).

Our LSTM networks consist of one (Elbe) or two (Weser) LSTM layers, and one fully connected dense layer to achieve the correct output dimension. The schematic is shown in Figure 3.

We split the hourly input data in chronological order −80% for training, 10% for validation, and 10% for testing—and evaluated the LSTM model performance on the unseen test set. When time series contain strong long-term trends, a random data split can sometimes yield a more robust assessment. This can be achieved by assembling the data sets for training, validation, and testing out of data segments from different temporal periods. This does not apply in our case, as our time series show no significant trends.

The networks were fine-tuned by adjusting several hyperparameters and evaluated for their respective performance. The performance of the network in the training process was assessed by computing the root mean square error (RMSE) between the predicted and actual values of the validation data set as well as the determination coefficient R^2. The network size was optimized by a stepwise change of the units (dimension of hidden state) from

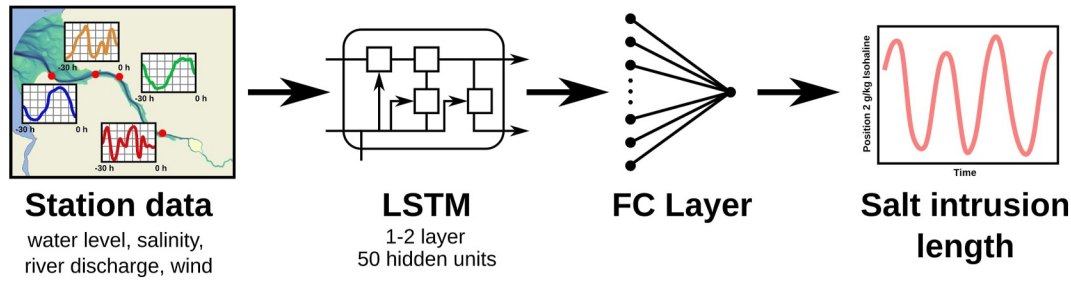

Figure 3. Schematic illustration of the structure of the used Long Short-Term Memory network including the input variables, the included layers, and the target variable.

10 to 100 and the number of LSTM layers from one to three. Tuning the units and number of layers showed the network's performance robustness to small changes in those parameters. Additionally, the initial learning rate and learning rate schedule as well as the choice of optimizer and batch size were varied and chosen based on the best performance on the validation data set. We used a learning rate callback during the training that halved the current learning rate if the validation loss did not improve for 5 consecutive epochs. Furthermore, we used early stopping as termination criteria if the validation loss did not improve for 10 consecutive epochs or the learning rate fell below 10^{-5}. Due to these mechanisms, the number of epochs necessary in the training process varies but was generally reduced to below 100 for both applications. It should be noted that we did not use the last network weights but chose the ones with the smallest validation error after the training process. The optimized hyperparameter settings are summarized in Table 2. The hyperparameters between both LSTM networks vary slightly primarily due to the different lengths of the training data sets.

In the first approach, the network estimates the subsequent time step, which denotes the anticipated salt intrusion length in the following hour. The LSTM network has the capacity to predict additional time steps. However, this can result in a decreased performance. This topic is further analyzed in Section 4.4.

3.4. Performance Metrics

We calculated different performance metrics to assess and compare our LSTM models' performance. The RMSE is defined as

$$RMSE = \sqrt{\frac{1}{N}\sum_{i=1}^{N}\left(y_{true,i} - y_{pred,i}\right)^2}, \tag{6}$$

with N being the total number of input samples and $y_{true,i}$ and $y_{pred,i}$ the true and predicted target values. The coefficient of determination R^2 is defined as

$$R^2 = \frac{\sum_{i=1}^{N}\left(y_{pred,i} - \bar{y}\right)^2}{\sum_{i=1}^{N}\left(y_{true,i} - \bar{y}\right)^2}, \tag{7}$$

with $\bar{y} = \frac{1}{N}\sum_{i=1}^{N} y_{true,i}$.

Table 2
LSTM Hyperparameters

Hyperparameter	Weser estuary	Elbe estuary
Available Data	52,441 days	12,433 days
Number of LSTM layer	2	1
Number of Hidden Units	50/50	50
Initial Learning Rate	0.001	0.001
Batch Size	64	32
Optimizer	Adam	Adam
Window Size	30 hr	30 hr

4. Results and Discussion

4.1. Network Performance on Simulated Data

To simplify the task, we first tested the LSTM networks on simulated data to assess how well the networks can reproduce the numerical model simulations. The performance of the networks on unseen test data is summarized in Table 3. Random weight initialization can introduce slight performance variability across identical networks. We trained 10 independent LSTM

Table 3
RMSE and R^2 for the Test Data of the Elbe and Weser Estuary Application for the Raw Prediction and 25 hr Rolling Mean

	RMSE (normalized)		RMSE (absolute) [m]		R^2	
Application	Raw	25 hr mean	Raw	25 hr mean	Raw	25 hr mean
Performance on Simulated Data						
Weser estuary	0.0307	0.0191	221	138	0.999	0.997
Elbe estuary	0.0503	0.0384	566	431	0.994	0.986
Performance on Observational Data						
Weser estuary	0.1483	0.1275	1,071	920	0.965	0.863
Elbe estuary	0.2013	0.1732	2,274	1,956	0.899	0.984

Note. The performance is evaluated for training on simulated data and actual observational data (compare Section 4.2. The relative error of the normalized variables and the absolute error are given in all applications.

models for the Weser estuary under the same settings to quantify this. The RMSE standard deviation was 0.001 in the normalized case and 10.4 m in the absolute case. Although these fluctuations do not affect the model's overall predictive capability, we consider them when comparing input features and their impact on performance (Section 4.3).

Test data time series of the predicted and given location of the 2 g/kg isohaline in the Weser estuary are displayed in Figure 4 and for the Elbe estuary in Figure 5. For both applications, two zooms on shorter periods are given to provide a more detailed view of the performance. We chose periods with different characteristics, that is, periods of high and low salt intrusion for the Weser estuary and a distinct salt intrusion extreme and a more variable period for the Elbe estuary to display the performance under different conditions.

In the Weser estuary, our LSTM network predicted salt intrusion length with an absolute RMSE of 221 m. Applying a 25 hr rolling mean further reduced the absolute RMSE to 138 m, demonstrating the model's robust performance in capturing subtidal dynamics.

For the Elbe estuary, the performance is slightly lower than for the Weser estuary with an absolute RMSE of 566 and 431 m (25 hr mean), respectively. The reduced number of training samples due to the shorter numerical model simulation can mainly explain this. We explore how training data volume affects LSTM performance in Section 4.4. Furthermore, the numerical model runs at a coarser resolution, producing a less accurate and temporally more uneven target variable. That makes the neural network's prediction task more challenging. It must be noted that different time periods are used for the estuaries due to the availability of the numerical model simulations. Although the measurement techniques have not changed and no drastic, persistent changes in the climatic conditions occurred during the evaluated time periods, the short-term hydrological, and climatic conditions can differ. This must be taken into account when comparing the results between the Elbe and Weser estuaries directly.

We further want to estimate the performance of the LSTM networks for the Weser and Elbe estuaries under varying conditions in particular low- and high discharge periods. Next to a scatterplot of given and predicted salt intrusion length, we evaluated the RMSE of individual salt intrusion zones in Figure 6. To this end, the test data were organized into bins of approximately equivalent size. The results obtained for the Weser estuary demonstrate slightly decreased performance in periods of high discharge with the salt front being located further downstream of approximately Weser-km 49. The scatterplot reveals a higher variability of the results in these regions. However, the results are in general well aligned. The results of the Elbe estuary differ from those of the Weser estuary. Except for the bin of most pronounced salt intrusion with strongly increased RMSE, the performances along the remaining range of intrusion lengths are uniform. The scatterplot indicates a general tendency of underestimation of the strong intrusion events (note that a higher predicted value means an underestimation due to the river kilometer increasing downstream). With the Elbe estuary having less training data available, the prediction of events at the extreme end of the spectrum is more difficult for the LSTM network.

The LSTM networks in this study can be trained without additional computational resources on a single device in under 1 hr (Processor description: Intel Corporation, 2025). The prediction on the whole test data set only takes a few seconds. This shows the greatest advantage of the networks—trained on the data of a model they can

10.1029/2025JH000768

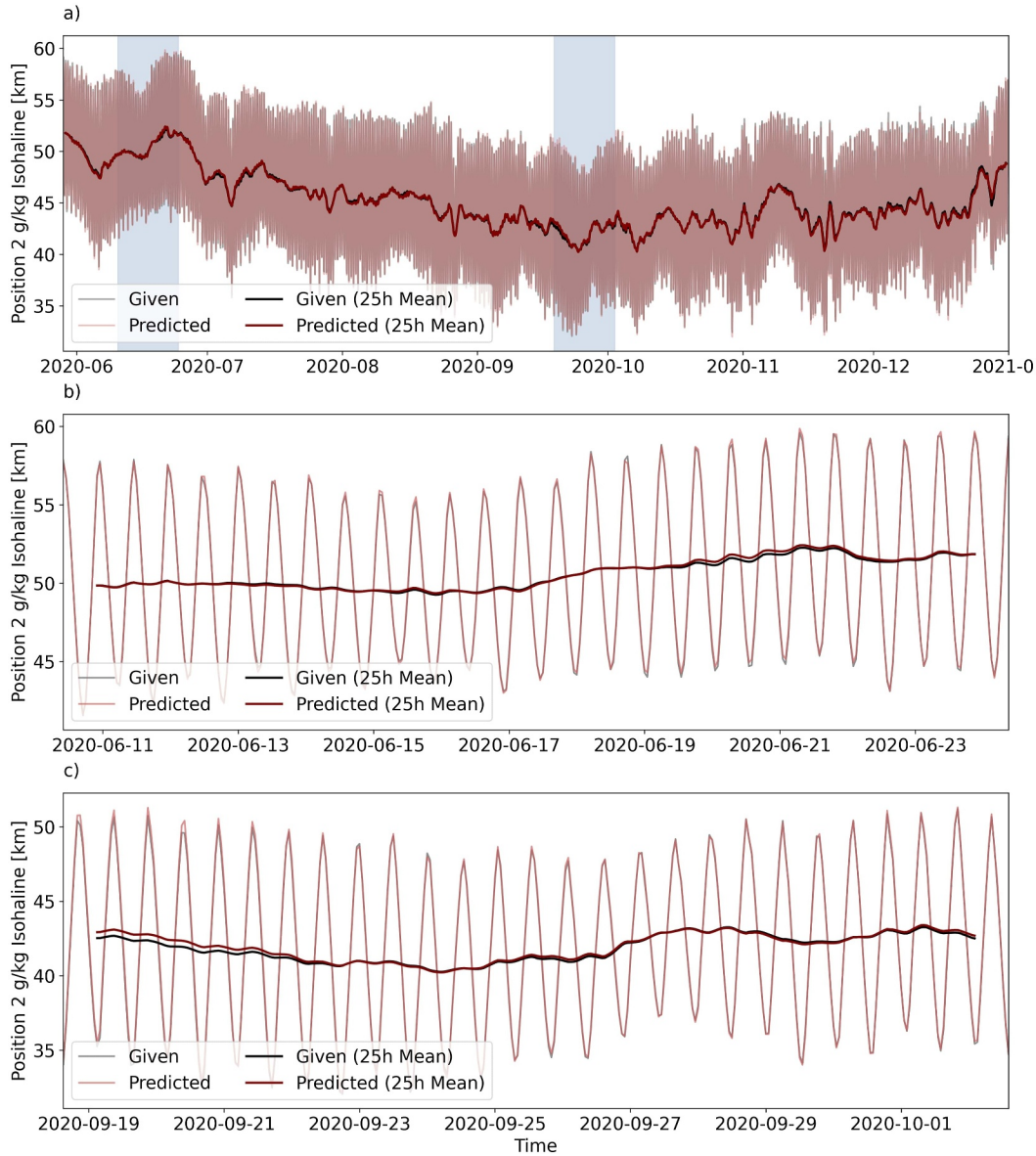

Figure 4. Given (black) and predicted (red) position of the 2 g/kg bottom isohaline along the Weser navigational channel for the whole test data (a) and two selected, zoomed-in periods (b, c). The periods in (b, c) are indicated in (a) by a light blue shading. The 25 hr tidal average for both time series is shown in bold lines.

reproduce this numerical model in seconds without having to run the numerical model. Real-time statements about the salt intrusion are possible using simple algorithms without the extensive computational resources of operational models.

To validate the use of LSTM networks, we tested a multivariate linear regression (MLR) and a classical feed-forward neural network (FFN) on the same input features and prediction task. Both showed less accurate prediction results, emphasizing the good performance of LSTM networks in applications with a temporal dimension. For the Weser estuary, the FFN achieved a normalized RMSE of 0.0486, an absolute RMSE of 351 m, and an R^2 score of 0.996, which is a good performance although worse than the LSTM. The error values of the linear regression were 0.1454, 1,022 m and 0.968. For the Elbe estuary, the FFN got a value of 0.0893 for the normalized RMSE, 1,003 m for the absolute RMSE, and an R^2 score of 0.982. The linear regression achieved error values of 0.1693, 1,867 m, and 0.943. For a further analysis of the performance of the LSTM against different model architectures, see Section Appendix B and Figure B1. None of the tested architectures showed better full-training

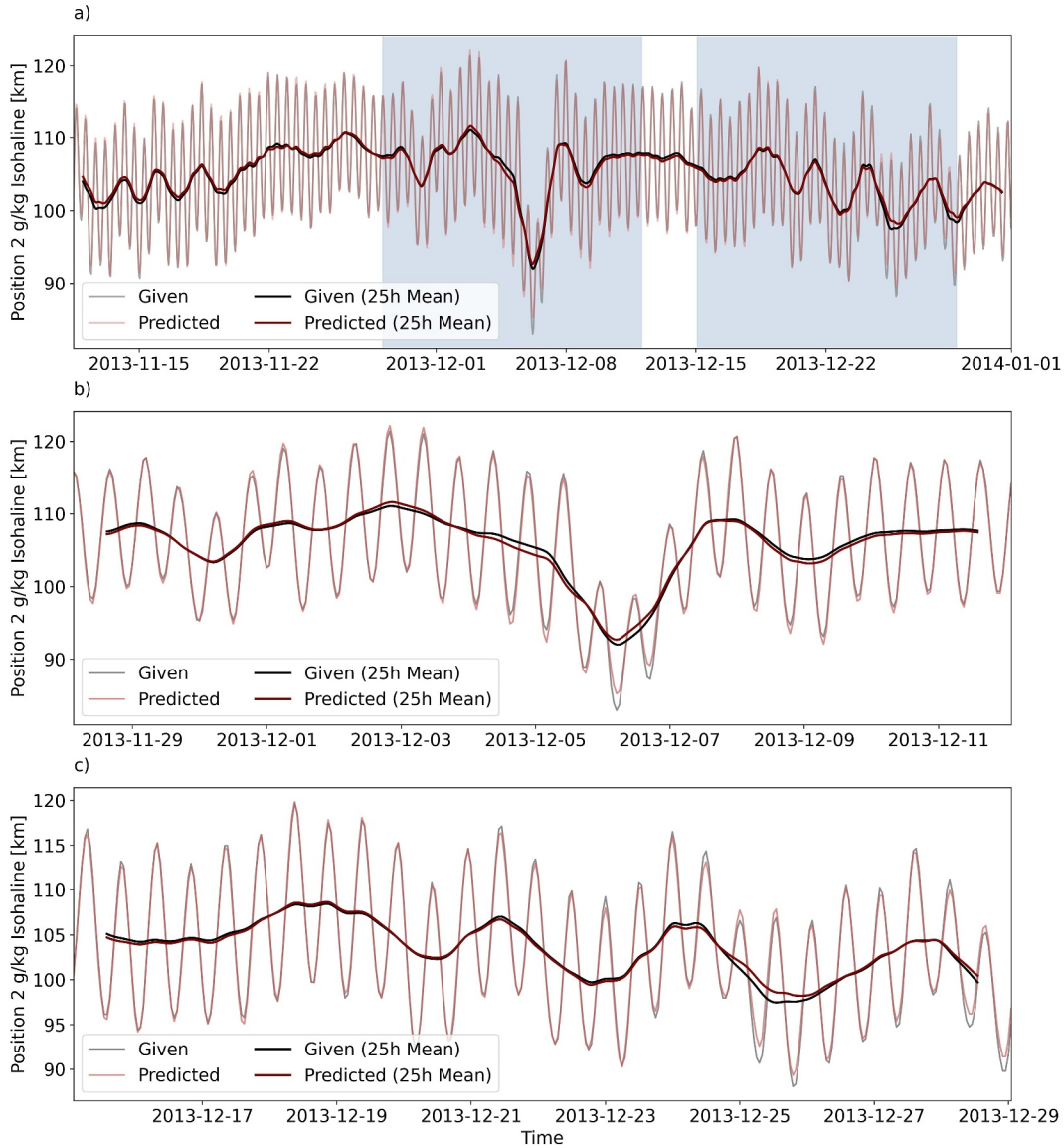

Figure 5. Given (black) and predicted (red) position of the 2 g/kg bottom isohaline along the Elbe navigational channel for the whole test data (a) and two selected, zoomed-in periods (b, c). The periods in (b, c) are indicated in (a) by a light blue shading. The 25 hr tidal average for both time series is shown in bold lines.

results than the LSTM, although the GRU performed slightly better on one to two training years. This suggests that this performance advantage depends on the application and quality of training data.

4.2. Network Performance on Observational Data

We further assessed the performance of LSTM networks on observational time series. The results show a decreasing performance in both applications and are included in Table 3. The decreased performance is largely due to the inaccuracy of the numerical model in salinity. The LSTM network is trained using a target variable derived from the simulation results. Consequently, the salinity station data from the same model simulation align perfectly with the simulated salt intrusion. Despite the model being calibrated and validated on the observational station data, discrepancies between the observational and simulated data are visible at specific points. This indicates that the observational station data do not perfectly align with the simulated target variable. As the errors in the numerical model are not a uniform bias that the LSTM can learn, the prediction task for the network becomes more difficult when trained on observational data. Therefore, the error of the LSTM, which was analyzed in

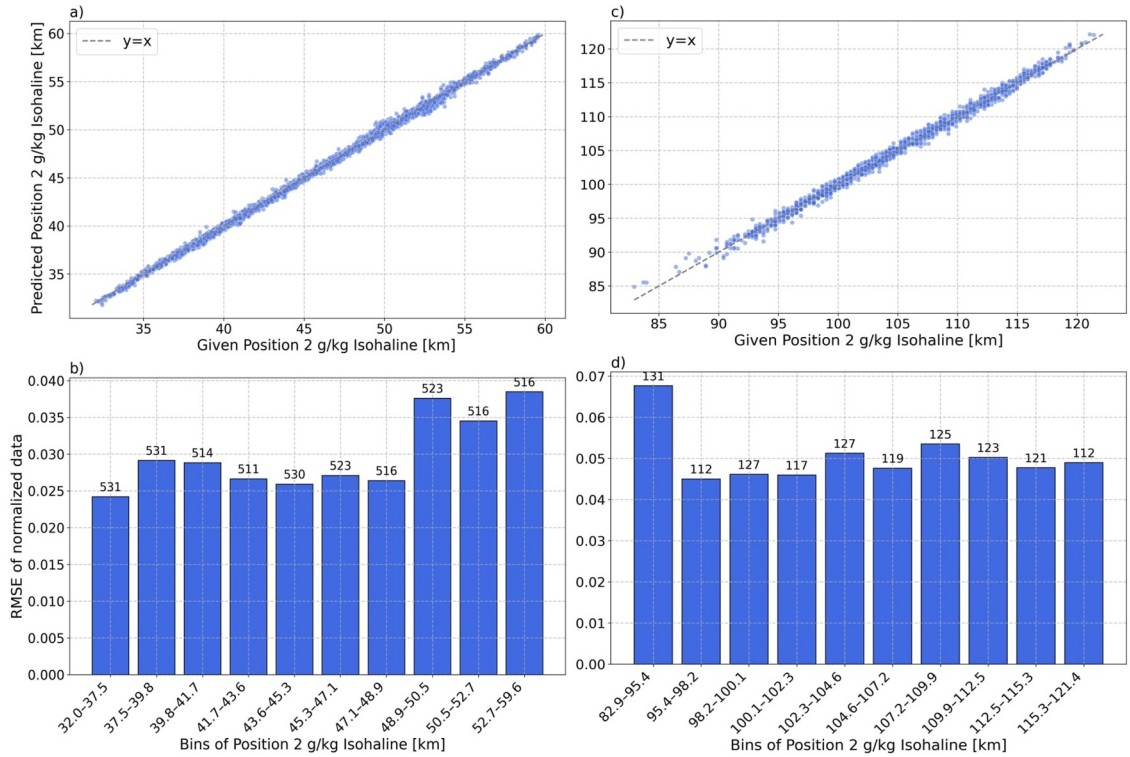

Figure 6. Scatterplot of the given and predicted position of the 2 g/kg bottom isohaline along the Weser (a) and Elbe (c) navigational channels. The root mean square error (RMSE) of the predicted position of the 2 g/kg bottom isohaline across different river kilometer ranges for the Weser (b) and Elbe (d) estuaries is shown. The RMSE is averaged over all data points included in the bin. The number of data points in each bin is noted in black directly above the respective bar. Note that the bin sizes are not perfectly equal due to test data points with nearly identical salt intrusion values.

Section 4.1, is added to the error of the numerical model itself. The numerical model of the Elbe estuary has a coarser resolution than the one of the Weser estuary, leading to less accurate simulation results for the position of the salt intrusion due to larger grid cells. In addition to the smaller training data set already causing worse performance, this is another factor leading to higher performance errors for this application. Otherwise, gaps in the observational data aggravate the performance loss for the Elbe estuary. Here, we excluded the affected periods, reducing the available data by more than 128 days. The gaps could be addressed with gap-filling algorithms that should not be part of this study. For possible mechanisms dealing with similar data, see, for example, Oehmcke et al. (2016). In the Weser estuary case, the input features' time series did not show gaps.

Nevertheless, the results for both applications are satisfactory and show that the trained network is applicable to measurement stations. However, the necessity for a good numerical model simulation as a basis for the training on the salt intrusion length becomes apparent. The neural network, trained on the numerical model, can rebuild the numerical results based on observation only to the degree of accuracy of the underlying numerical model simulation.

4.3. Feature Sensitivity

When using measurement data, gaps in the time series can occur frequently, for example, due to failing sensors. As an alternative to the gap-filling mechanisms method, we want to test the possibility of changing input stations or leaving specific stations or data completely out of the LSTM network for our applications. This also gives insights into the importance of specific features for the prediction of the network. For this analysis, we concentrated on the Weser estuary application. An analogous analysis for the Elbe estuary is not shown here, as less training data are available and the scenarios and results are qualitatively similar to those of the Weser estuary due to their strong similarities.

Table 4
RMSE and R^2 for the Test Data of the Weser Estuary Feature Sensitivity Scenarios

Scenario	RMSE (normalized)	RMSE [m] (absolute)	R^2
Exchanged input features (mod data)	0.0315 (+2.6%)	227	0.998
Exchanged input features (obs data)	0.1758 (+16.4%)	1,258	0.950
Outer Weser stations (mod data)	0.0730 (+137.8%)	526	0.992
Outer Weser stations (obs data)	0.1902 (+26.0%)	1,370	0.938
No discharge data (mod data)	0.0320 (+4.2%)	231	0.998
No discharge data (obs data)	0.1842 (+22.0%)	1,329	0.945
No wind data (mod data)	0.0300 (−2.3%)	216	0.999
No wind data (obs data)	0.1658 (+9.8%)	1,196	0.954

Note. For all scenarios, one LSTM network was trained each on the simulated data and the observational data. The relative error of the normalized variables and the absolute error are given. The change of the normalized RMSE in comparison to the baseline experiments in Sections 4.1 and 4.2 in percent is given in brackets.

We created different scenarios imitating issues that could be expected in reality and trained new LSTM networks on the adapted set of input features. The results are compared to the original scenario of Section 4.1. It must be noted that for these experiments, the hyperparameters of the network were not individually optimized anew. We used the original network's settings, which could lead to small biases as the input dimension changes with fewer input features. However, as the hyperparameter tuning of the original network showed a robustness of the network's performance to small changes in the dimension of the network (number of units and layers), we expect these biases to be rather small.

We identified four potential data failures—salinity and water-level stations, discharge gauges, and wind sensors—and tested their impact. We removed those inputs from the data sets to simulate discharge and wind sensor outages. To emulate salinity or water-level station failures, we ran two experiments: (a) distributed substitution: we replaced the failed stations with an alternative set of sensors still spanning the entire estuary. Moreover, (b) outer-estuary only: we used data exclusively from stations in the Outer Weser estuary to evaluate how the LSTM performs when limited to high-salinity inputs.

As explained in Section 3.1, the input features of the LSTM networks for the Weser estuary have a correlation of less than 80 % among themselves (compare Figure A1). This implies that stations could be exchanged with different correlated stations in case of sensor failure. It could still be possible to predict the salt intrusion with a similar level of accuracy.

In the exchanged input features scenario with a distributed substitution, we trained new LSTM networks, replacing the water level stations of Table 1 with "Dwarsgat" and "Brake" and the salinity stations with "Dwarsgat," "Nordenham," and "Brake" for both applications on simulated and observational data. The Weser River discharge and wind measurements are still included. The results of the scenarios are given in Table 4 both for training on simulated and observational data. In the case of the training on simulated data, there are no big performance differences from the original scenario, supporting the interchangeability of the stations. The error occurring is inside the range of the network's variability mentioned in Section 4.1. For training on observational data, the error is comparatively higher. This suggests that, in this case, the replacement measurement stations are not as good for the prediction as the originally chosen stations.

In realistic usage, replacing single stations is, of course, also possible and should be the preferred act in case of one station's failure. We here exchanged all stations for proof of concept.

Next, in the Outer Weser stations scenarios, we wanted to test the performance of the LSTM network by just using input features located in the downstream part of the estuary. This tests the ability of the method in situations without having measurement stations in areas of low salinity and thus in close proximity to the target. For that, we trained the network on the water level and salinity of the stations "Dwarsgat" and "Bremerhaven" in the Outer Weser estuary. In the given observational data, these stations have a mean salinity of around 26 and 12 g/kg, respectively. For the network trained on simulated data, the performance decreased a lot compared to the original

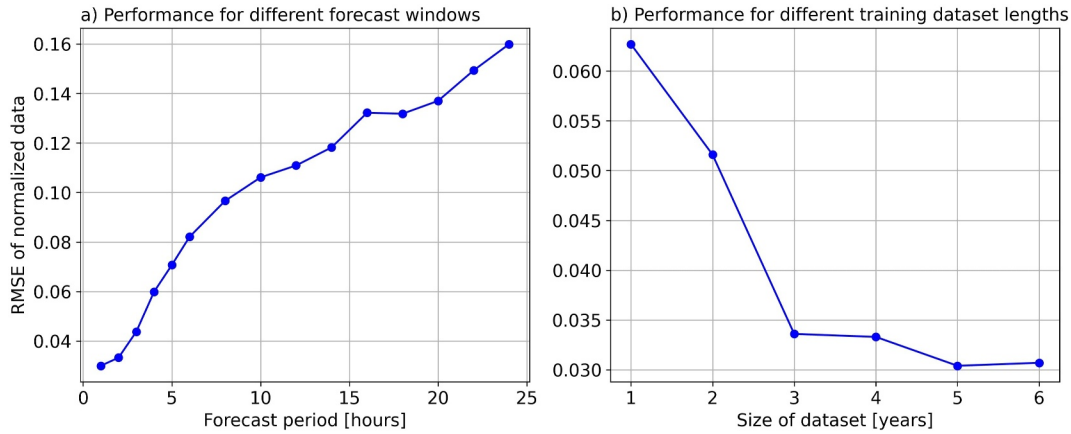

Figure 7. Root mean square error values between the given and predicted time series of the normalized test data for different forecast periods and data set sizes in the Weser estuary application.

model while still giving relatively good results compared to different scenarios or applications. The performance loss is much smaller for the network trained on the observational data. This indicates that when training on observational data, the Lower Weser stations are not taken into account as much as when training on simulated data. The results in this scenario align with results by Lauer and Kösters (2024), who described the loss in performance caused by the increased distance between input features and target variables.

The third tested scenario excludes the Weser River discharge input feature. Although the discharge is one of the biggest drivers of the salt intrusion, leaving it out reduces the accuracy of the network on unseen data when trained on simulated data only by a small amount that lies within the range of the network's variability. In the case of the performance on observational data, this is different, as the performance decreases by more than 20 %. This variation suggests that when using the observational data, the discharge is taken more into account by the network due to the error of the numerical model and the resulting difference between the measurement stations and the modeled target variable.

In addition to the previous results of the high-salinity station (Outer Weser stations) scenario, the exclusion of the Weser River discharge indicates that the importance of input features shifts between training on simulated or observational data. The training on observational data relies more on discharge data, and the training on simulated data relies on the features from the low-salinity stations. This substantiates the importance of a good numerical model producing the target variable data, as the network trained on the simulated data relies on its performance on the good alignment between the low-salinity stations and the salt intrusion front in the model.

Lastly, in the no wind data scenario, we tested the effect of omitting the wind data features from the station "Bremen".

Training the LSTM on simulated data even improved its performance although, the gain remained within the network's normal variability. When we trained on observational data, performance dropped by less than 10 %. These findings indicate that wind measurements do not meaningfully enhance salt intrusion forecasts since water level data and other inputs already convey the necessary information.

4.4. Forecasting Window and Dependence on Training Data Size

Although this study is focused on the direct approximation of the salt inflow quantities, it is also possible to make further projections for the future. It should be noted that the LSTM networks were not specifically trained for this task but just adapted to predict more than one step.

For the Weser estuary, the accuracy of predictions up to 24 hr in advance is shown in Figure 7a with training on simulated data. With a longer forecast period, the normalized RMSE increases and the performance drops continuously. This suggests that the salt intrusion length in this application is highly dependent on short-term changes in the behavior of the input features, making a long-term prediction more difficult. Despite the decrease in accuracy, the prediction 24 hr ahead with a RMSE of 0.1599, equivalent with an absolute error below

1,200 m, is useful for warning systems. A decrease in prediction performance with longer forecast periods was also seen in results by Wullems et al. (2023) and Saccotelli et al. (2024). In both studies, the networks were trained on daily data and used to predict salinity up to 7 days ahead. Their prediction is based on a different timescale especially not including tidal variations and only focusing on subtidal tendencies. Else, the studies concentrate on the prediction at a specific location without spatial information. Therefore, the studies are not directly comparable to ours but confirm the difficulties of long-term predictions.

The LSTM network generally showed higher prediction errors for the Elbe application than for the Weser primarily caused by the smaller training data set available. Neural network performance typically benefits from larger training data sets (Goodfellow et al., 2016); however, the data needed strongly depend on the particular use case. To assess the dependence on the number of training data and to give estimates of how much data has to be collected to give reliable results, we trained the Weser estuary network on different numbers of training years. The validation and test data set thereby stayed the same to reduce the bias, and the training data were reduced according to the number of years included in the data set. The results can be seen in Figure 7b.

For this specific application, a 3-year training data set gives almost the same results as a 6-year data set. However, the results for one or 2 years of data are significantly worse than for the longer training period, although the overall performance is still good. This aligns with the Elbe estuary results, which were produced on less than 1.5 years of training data and gave a normalized RMSE of 0.0545.

Although this is highly dependent on the choice of application, it could give a rough measure of the amount of training data needed to achieve corresponding results. We expect that for more complex estuaries, for example, nontidal estuaries, which are more dependent on longer timescales, a longer time period of training data is necessary.

5. Conclusion

This study presented LSTM networks as a suitable tool for estuarine salt intrusion prediction. Trained on a numerical model, the network can reproduce the model results solely on the basis of a few measurement stations. The long and expensive numerical model runs can be substituted by predictions that only take a few seconds. This simplifies the assessment of the salt dynamics inside the estuary in real time—leveraging and accelerating decision-making regarding coastal protection and other socioeconomic threats. For the first time, we applied this method to the Weser and Elbe estuaries as examples of highly dynamic tidal estuaries. Going beyond previous studies, we are not approximating variables at specific locations but rather predicting the position and movement of the target variable.

Although the performance of the networks was more accurate in the Weser estuary mainly due to the higher amount of available training data, the predictions also show a good alignment in the Elbe estuary. When trained solely on observational data and not on simulated data corresponding to measurement stations, the performance decreases due to the error of the numerical model. This is caused by the target variable—the salt intrusion length—being solely derived from the numerical model, as it cannot be continuously observed in reality. This emphasizes the need for a good numerical model to predict the salt intrusion length. Despite the fact that both applications demonstrate relatively good performance across a range of salt intrusion lengths, weaknesses become evident during events of salt intrusion at the extremes of the spectrum particularly in the case of the Elbe estuary with less training data. The LSTM's ability could not be tested under pronounced extreme events because no such events occurred during the available numerical simulation period.

In feature sensitivity studies, we showed that similar results can be achieved even in the case of station failure or other missing input features. Not all available stations are needed especially in the highly monitored estuaries such as the Weser and Elbe. Therefore, a failing station can be replaced by a correlated one without losing accuracy. This indicates that this method can also work in less monitored estuaries where not as many measurement stations are available and the input stations are located further away from the target variable position. We highlight this approach's limitations for extended forecasts. Because estuarine salinity responds strongly to short-term environmental fluctuations, prediction accuracy declines as the lead time increases. Moreover, the LSTM requires substantial training data to sustain reliable long-range forecasts.

Nevertheless, we could show the suitability of LSTM networks for real-time predictions of estuarine salt intrusion in two different applications. In this study, the LSTM networks are used in an offline setting but they can be

embedded in online data flows and deliver the real-time information to relevant stakeholders. Due to the possibility of generalization, this method can easily be adapted to other estuaries or even to forecast other variables—given the numerical model and training data are available. The LSTM networks can be used for estuaries around the world and can advance coastal protection and warning mechanisms.

Appendix A: Correlation of Input Stations

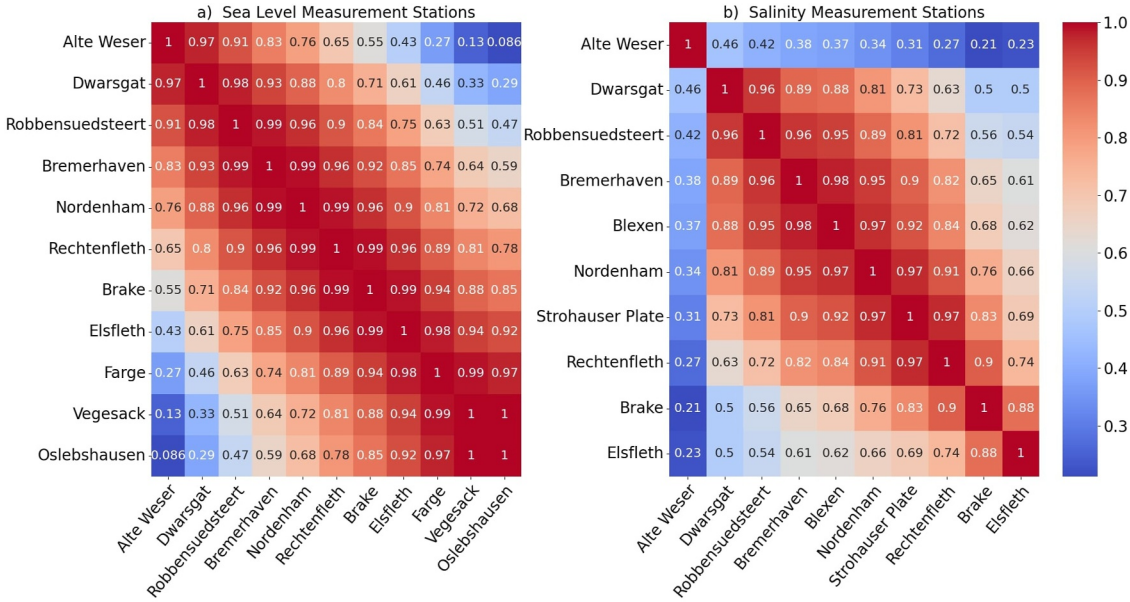

Figure A1. Heat map of the correlations between the numerical model results at the water level (a) and salt (b) measurement stations along the Weser estuary.

Appendix B: Model Comparison Across Different Training Data Sizes

Here, we validate the choice of LSTM networks and evaluate further possible model alternatives in data-limited applications. For that, we compare the performance of the LSTM network as presented in Figure 7 with different baseline models. These include an MLR, a support vector regression (SVR), a classical feedforward neural network (FFN), and a gated recurrent unit network (GRU, Cho et al., 2014).

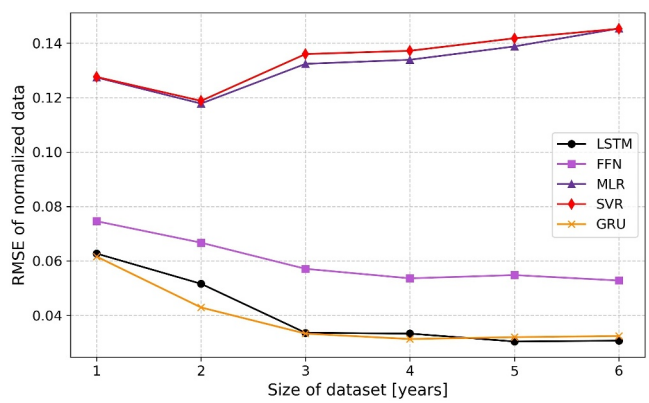

Figure B1. Root mean square error values between the given and predicted time series of the normalized test data for different models on different data set sizes in the Weser estuary application.

The MLR and SVR demonstrate similar performance along the range of training data set sizes. Although they have a much larger RMSE compared to the other network architectures, they demonstrate better performance on reduced input data. The GRU and LSTM networks exhibit very similar results. The GRU appears to work slightly better with reduced input data while having a slightly lower performance on bigger data sets with the differences partly being inside the range of the network's internal variability. The performance advantage of the GRU with small training data sets could not be confirmed in the Elbe estuary case (not shown here), suggesting a dependence on the application and training data quality.

Conflict of Interest

The authors declare no conflicts of interest relevant to this study.

Data Availability Statement

All python scripts and data needed to run the experiments described in this manuscript are published at https://doi.org/10.5281/zenodo.16500183 (Rummel, 2025).

Acknowledgments
The work of Karoline Rummel is supported by the Research and Development Project "Saline" (B3955.02.06.10018) funded by the Federal Waterways Engineering and Research Institute. The authors would like to thank the Computational Intelligence Technology Lab team under the lead of Prof. Dr. Roger Labahn (University of Rostock, Institute for Mathematics) for support and valuable discussions about implementing machine learning algorithms. We also want to thank Prof. Dr. Klaus Neymeyr (University of Rostock, Institute for Mathematics) for the financial support of Karoline Rummel at the very beginning of this work. Further, we want to thank Lloyd Reese (Leibniz-Institute for Baltic Sea Research Warnemünde) for providing the Elbe estuary numerical model data. We are grateful for the comments from three anonymous reviewers. Open Access funding enabled and organized by Projekt DEAL.

References

Alizadeh, M. J., Kavianpour, M. R., Danesh, M., Adolf, J., Shamshirband, S., & Chau, K.-W. (2018). Effect of river flow on the quality of estuarine and coastal waters using machine learning models. *Engineering Applications of Computational Fluid Mechanics*, *12*(1), 810–823. https://doi.org/10.1080/19942060.2018.1528480

Bellafiore, D., Ferrarin, C., Maicu, F., Manfè, G., Lorenzetti, G., Umgiesser, G., et al. (2021). Saltwater intrusion in a mediterranean Delta under a changing climate. *Journal of Geophysical Research: Oceans*, *126*(2), e2020JC016437. https://doi.org/10.1029/2020jc016437

Boehlich, M. J., & Strotmann, T. (2008). The Elbe Estuary. *Die Küste*, *74*(1), 288–306.

Burchard, H., & Bolding, K. (2002). GETM–A general estuarine transport model. *Tech. Rep. EUR*. JRC23237S.

Burchard, H., Bolding, K., & Villarreal, M. R. (1999). GOTM, a general ocean turbulence model: Theory, implementation and test cases. *Tech. Rep. EUR*, *18745*, 103.

Cho, K., Van Merriënboer, B., Gulcehre, C., Bahdanau, D., Bougares, F., Schwenk, H., & Bengio, Y. (2014). Learning phrase representations using rnn encoder-decoder for statistical machine translation. *arXiv preprint arXiv:1406.1078*.

Costa, Y., Martins, I., de Carvalho, G. C., & Barros, F. (2023). Trends of sea-level rise effects on estuaries and estimates of future saline intrusion. *Ocean and Coastal Management*, *236*, 106490. https://doi.org/10.1016/j.ocecoaman.2023.106490

Fang, L., & Shao, D. (2022). Application of long short-term memory (LSTM) on the prediction of rainfall-runoff in karst area. *Frontiers in Physics*, *9*, 790687. https://doi.org/10.3389/fphy.2021.790687

German Meteorological Service (DWD). (2025). Wind measurement data at stations cuxhaven and Bremen. Retrieved from https://opendata.dwd.de/

Goodfellow, I., Bengio, Y., Courville, A., & Bengio, Y. (2016). Deep learning. *MIT press Cambridge*, *1*(2).

Gorski, G., Cook, S., Snyder, A., Appling, A. P., Thompson, T., Smith, J. D., et al. (2024). Deep learning of Estuary salinity dynamics is physically accurate at a fraction of hydrodynamic model computational cost. *Limnology & Oceanography*, *69*(5), 1070–1085. https://doi.org/10.1002/lno.12549

Guillou, N., Chapalain, G., & Petton, S. (2023). Predicting sea surface salinity in a tidal Estuary with machine learning. *Oceanologia*, *65*(2), 318–332. https://doi.org/10.1016/j.oceano.2022.07.007

Hochreiter, S., & Schmidhuber, J. (1997). Long short-term memory. *Neural Computation*, *9*(8), 1735–1780. https://doi.org/10.1162/neco.1997.9.8.1735

Hu, J., Liu, B., & Peng, S. (2019). Forecasting salinity time series using RF and ELM approaches coupled with decomposition techniques. *Stochastic Environmental Research and Risk Assessment*, *33*(4–6), 1117–1135. https://doi.org/10.1007/s00477-019-01691-1

Intel Corporation. (2025). Intel® Core™ i7-8550U processor @1.8 GHz x 8. Retrieved from https://www.intel.com/content/www/us/en/products/sku/122589/intel-core-i78550u-processor-8m-cache-up-to-4-00-ghz/specifications.html

Jörges, C., Berkenbrink, C., & Stumpe, B. (2021). Prediction and reconstruction of ocean wave heights based on bathymetric data using LSTM neural networks. *Ocean Engineering*, *232*, 109046. https://doi.org/10.1016/j.oceaneng.2021.109046

Klingbeil, K., Lemarié, F., Debreu, L., & Burchard, H. (2018). The numerics of hydrostatic structured-grid coastal ocean models: State of the art and future perspectives. *Ocean Modelling*, *125*, 80–105. https://doi.org/10.1016/j.ocemod.2018.01.007

Kösters, F., Grabemann, I., & Schubert, R. (2014). On SPM dynamics in the turbidity maximum zone of the Weser Estuary. *Die Küste*, *81*, 393–408.

Kratzert, F., Klotz, D., Brenner, C., Schulz, K., & Herrnegger, M. (2018). Rainfall–runoff modelling using long short-term memory (LSTM) networks. *Hydrology and Earth System Sciences*, *22*(11), 6005–6022. https://doi.org/10.5194/hess-22-6005-2018

Lange, D., Müller, H., Piechotta, F., & Schubert, R. (2008). The Weser Estuary. *Die Küste*, *74*, 275–287.

Lauer, F., & Kösters, F. (2024). Using statistical and machine learning approaches to describe estuarine tidal dynamics. *Journal of Hydroinformatics*, *26*(4), 853–868. https://doi.org/10.2166/hydro.2024.294

Lee, J., Biemond, B., de Swart, H., & Dijkstra, H. A. (2024). Increasing risks of extreme salt intrusion events across European estuaries in a warming climate. *Communications Earth and Environment*, *5*(1), 60. https://doi.org/10.1038/s43247-024-01225-w

Luo, Q.-R., Xu, H., & Bai, L.-H. (2022). Prediction of significant wave height in hurricane area of the Atlantic Ocean using the Bi-LSTM with attention model. *Ocean Engineering*, *266*, 112747. https://doi.org/10.1016/j.oceaneng.2022.112747

Niedersächsischer Landesbetrieb für Wasserwirtschaft, Küsten- und Naturschutz (NLWKN). (2015). Deutsches gewässerkundliches jahrbuch weser-und emsgebiet 2015. Retrieved from https://www.nlwkn.niedersachsen.de/startseite/wasserwirtschaft/publikationen/deutsches_gewasserkundliches_jahrbuch/deutsches-gewaesserkundliches-jahrbuch-weser-und-emsgebiet-43607.html

Niedersächsischer Landesbetrieb für Wasserwirtschaft, Küsten- und Naturschutz (NLWKN) Verden. (2023). *Measurement stations Hellwege, Hexenberg OW, Grasberg (HELL, HEX, GRAS). Waterways and shipping administration*. Provided by Federal Waterways Engineering and Research Institute.

Oehmcke, S., Zielinski, O., & Kramer, O. (2016). kNN ensembles with penalized DTW for multivariate time series imputation. In *2016 international joint conference on neural networks (ijcnn)* (pp. 2774–2781).

Reese, L., Gräwe, U., Klingbeil, K., Li, X., Lorenz, M., & Burchard, H. (2024). Local mixing determines spatial structure of diahaline exchange flow in a mesotidal Estuary–A study of extreme runoff conditions. *Journal of Physical Oceanography*, *54*(1), 3–27. https://doi.org/10.1175/jpo-d-23-0052.1

Rohmer, J., & Brisset, N. (2017). Short-term forecasting of saltwater occurrence at La Comté River (French Guiana) using a kernel-based support vector machine. *Environmental Earth Sciences*, *76*, 1–16.

Rummel, K. (2025). Python Files and Datasets from Rummel et al.: Real-Time Prediction of Salt Intrusion in Tidal Estuaries using Long Short-Term Memory Networks. *Zenodo*. https://doi.org/10.5281/zenodo.16500183

Rummel, K., Gräwe, U., Klingbeil, K., Kolb, P., Li, X., Reese, L., & Burchard, H. (2025). Spatially resolved salt intrusion mechanisms in a tidal Estuary and the impact of channel deepening. *Journal of Geophysical Research: Oceans*, *130*(6), e2024JC022073. https://doi.org/10.1029/2024jc022073

Saccotelli, L., Verri, G., De Lorenzis, A., Cherubini, C., Caccioppoli, R., Coppini, G., & Maglietta, R. (2024). Enhancing Estuary salinity prediction: A machine learning and deep learning based approach. *Applied Computing and Geosciences*, *23*, 100173. https://doi.org/10.1016/j.acags.2024.100173

Sherstinsky, A. (2020). Fundamentals of recurrent neural network (RNN) and long short-term memory (LSTM) network. *Physica D: Nonlinear Phenomena*, *404*, 132306. https://doi.org/10.1016/j.physd.2019.132306

Sola, J., & Sevilla, J. (1997). Importance of input data normalization for the application of neural networks to complex industrial problems. *IEEE Transactions on Nuclear Science*, *44*(3), 1464–1468. https://doi.org/10.1109/23.589532

Strotmann, T. (2014). *Deutsches Gewässerkundliches Jahrbuch: Elbegebiet, Teil III: Untere Elbe ab der Havelmündung, 2012, Freie und Hansestadt Hamburg*. HPA Hamburg Port Authority. Retrieved from https://dgj.de/docs/eiii_2012.pdf.180

Strotmann, T. (2015). *Deutsches Gewässerkundliches Jahrbuch: Elbegebiet, Teil III: Untere Elbe ab der Havelmündung, 2013, Freie und Hansestadt Hamburg*. HPA Hamburg Port Authority. Retrieved from https://dgj.de/docs/eiii_2013.pdf.179

Tian, Q., Gao, H., Tian, Y., Wang, Q., Guo, L., & Chai, Q. (2024). Attribution analysis and forecast of salinity intrusion in the modaomen Estuary of the Pearl River Delta. *Frontiers in Marine Science*, *11*, 1407690. https://doi.org/10.3389/fmars.2024.1407690

Umlauf, L., & Burchard, H. (2005). Second-order turbulence closure models for geophysical boundary layers. A review of recent work. *Continental Shelf Research*, *25*(7–8), 795–827. https://doi.org/10.1016/j.csr.2004.08.004

Wang, N., & Ge, J. (2025). Predictions of saltwater intrusion in the changjiang Estuary: Integrating machine learning methods with fvcom. *Journal of Hydrology*, *653*, 132739. https://doi.org/10.1016/j.jhydrol.2025.132739

Waterways and Shipping Administration Elbe. (2025a). Measurement station neu darchau. Retrieved from https://www.kuestendaten.de/DE/Services/Messreihen_Dateien_Download/Download_Zeitreihen_node.html

Waterways and Shipping Administration Elbe-Nordsee. (2025b). Measurement stations–Sea level: Cuxhaven steubenhöft, brokdorf, glückstadt, stadersand, Schlau, Hamburg St Pauli and salinity: Cuxhaven alte liebe. *LZ2a Neufeldreede, LZ1b Krummendeich, D4 Rhinplate Nord*. Retrieved from https://www.kuestendaten.de/DE/Services/Messreihen_Dateien_Download/Download_Zeitreihen_node.html

Waterways and Shipping Administration Hamburg. (2025). Conductivity monitoring network in the tidal elbe. Retrieved from https://www.kuestendaten.de/Tideelbe/DE/Service/Leitfaehigkeitsmessnetz/Leitfaehigkeitsmessnetz_node.html

Waterways and Shipping Administration Hann. Muenden. (2023). *Measurement station intschede (INT)*. Provided by Federal Waterways Engineering and Research Institute.

Waterways and Shipping Administration Weser-Jade-Nordsee. (2023a). *Measurement station hemelingen (HEM)*. Provided by Federal Waterways Engineering and Research Institute.

Waterways and Shipping Administration Weser-Jade-Nordsee. (2023b). *Measurement station oberwasser hunte (OWH)*. Provided by Federal Waterways Engineering and Research Institute.

Waterways and Shipping Administration Weser-Jade-Nordsee. (2024). Measurement stations BHV alter leuchtturm, blexen, brake, dwarsgat, elsfleth, farge, leuchtturm alte weser, nordenham, oslebshausen, rechtenfleth, robbensuedsteert, strohauser plate. *Vegesack*. Retrieved from https://www.kuestendaten.de/DE/Services/Messreihen_Dateien_Download/Download_Zeitreihen_node.html

Wullems, B. J., Brauer, C. C., Baart, F., & Weerts, A. H. (2023). Forecasting estuarine salt intrusion in the rhine–meuse Delta using an LSTM model. *Hydrology and Earth System Sciences*, *27*(20), 3823–3850. https://doi.org/10.5194/hess-27-3823-2023

Zheng, R., Sun, Z., Jiao, J., Ma, Q., & Zhao, L. (2024). Salinity prediction based on improved lstm model in the qiantang Estuary, China. *Journal of Marine Science and Engineering*, *12*(8), 1339. https://doi.org/10.3390/jmse12081339